Polymer Chemistry

Exploring the Effects of Glyco-copolymer Architectures on the Solution Self-assembly of Amphiphilic Thermoresponsive Linear, Star, and Cyclic Polymers

Journal:	*Polymer Chemistry*
Manuscript ID	PY-ART-06-2023-000729.R1
Article Type:	Paper
Date Submitted by the Author:	25-Jul-2023
Complete List of Authors:	Ozawa, Naoki; Shinshu Daigaku Lee, Ji Ha; Hiroshima University, Department of Chemical Engineering, Graduate School of Advanced Science and Engineering Akiba, Isamu; University of Kitakyushu, Chemistry Nishimura, Tomoki; Shinshu Daigaku, Department of Chemistry and Materials, Faculty of Textile Science and Technology

ARTICLE

Exploring the Effects of Glyco-copolymer Architectures on the Solution Self-assembly of Amphiphilic Thermoresponsive Linear, Star, and Cyclic Polymers

Received 00th January 20xx,
Accepted 00th January 20xx

DOI: 10.1039/x0xx00000x

Naoki Ozawa,[a] Ji Ha Lee,[b] Isamu Akiba,[c] and Tomoki Nishimura *[a]

Polymer architecture can influence the morphology of polymer self-assemblies. However, although the ability to control the nanostructure of self-assemblies is crucial for optimizing their potential applications, the ways in which changes in macromolecular architecture affect the structures of self-assemblies and the conformation of polymer chains in self-assemblies remain virtually unknown. Herein, we investigate the self-assembly behavior of four amphiphilic copolymers with different chain configurations, namely, AB, ABA, 3-arm block copolymers, and cyclic graft copolymers. We demonstrate that changes in the macromolecular architecture can result in the formation of different nanostructures, including unilamellar vesicles, cylindrical micelles, spherical micelles, and multilamellar vesicles. X-ray and light-scattering measurements also reveal that the conformations of the polymer chains in the self-assemblies are different, which contributes to the differences in their nanostructures. Our findings provide insights into the ways in which changes in polymer architecture affect self-assembly behavior and suggest that the macromolecular architecture should be considered an important factor for controlling the structure of molecular assemblies.

Introduction

Controlling the morphology of polymer self-assemblies in solution is important, because their morphology can have a significant effect on their physical and chemical properties, which in turn affect their potential applications.[1, 2, 3, 4, 5] The nanostructures of molecular assemblies are therefore designed for specific purposes. For example, spherical micelles and vesicles have hydrophobic or hollow spaces that can encapsulate drugs for delivery to disease sites.[6, 7, 8] Cylindrical micelles are used as templates with a specific periodicity and orientation for nanolithography.[9, 10] The nanostructure of molecular assemblies can also influence their biological properties, such as recognition by cells and flow through blood vessels. This can be important in applications such as drug delivery, where the interactions between self-assemblies and cells, as well as their recognition by cells (e.g., dendric cells or macrophages), can influence their ability to circulate in the blood and accumulate at tumors.[11, 12] Given the importance of the nanostructure of polymer self-assemblies, it is hardly surprising that there has been considerable research into controlling their nanostructures. For example, Liu *et al*. prepared four different nanostructures including spheres, vesicles, discs and lamellae based on the self-assembly of amphiphilic block copolymers consisting of poly(ethylene glycol) and polymerised block of reduction-responsive camptothecin prodrug monomer by varying solvent compositions and demonstrated that lamellae structure exhibited extended blood circulation over other nanostructures.[13] More recently, the same research group has developed a new method for identifying and quantifying synthetic polymers in biological environments using sequence-defined amphiphilic polymers that form 'digital micelles' with different nanostructures. These micelles can be read using MALDI-TOF mass spectrometry, which also allows quantitative analysis, and this method has allowed the identification, decoding and quantification of different types of micelles at different biological levels.[14, 15]

The nanostructure of polymer self-assemblies is generally controlled by tailoring the polymer structures, such as the length of the hydrophilic and hydrophobic segments. The self-assembled structures are determined by the geometry of the amphiphiles in the molecular assembly, which can be described by the packing parameter.[16, 17, 18, 19] Therefore, for structurally simple AB-type amphiphilic block copolymers, we can fabricate molecular assemblies with different morphologies by changing the degree of polymerization or the composition of the hydrophilic and hydrophobic segments according to the packing-parameter rule. Among the factors in polymer structure, polymer architectures, such as branching, also influence the self-assembled structures.[20, 21, 22, 23, 24, 25, 26, 27, 28, 29, 30, 31, 32, 33, 34] For example, amphiphilic star and cyclic copolymers

[a] Department of Chemistry and Materials, Faculty of Textile Science and Technology, Shinshu University, 3-15-1, Tokida, Ueda, Nagano 386-8567, Japan
E-mail: nishimura_tomoki@shinshu-u.ac.jp
[b] Chemical Engineering Program, Graduate School of Advanced Science and Engineering, Hiroshima University, 1-4-1 Kagamiyama, Higashi-Hiroshima 739-8527, Japan
[c] Department of Chemistry and Biochemistry, University of Kitakyushu, 1-1 Hibikino, Kitakyushu, Fukuoka 808-0135, Japan
Electronic Supplementary Information (ESI) available: [details of any supplementary information available should be included here]. See DOI: 10.1039/x0xx00000x

not only exhibit changes in critical micelle concentration (CMC) and phase-transition temperature compared to the corresponding AB-type block copolymers, but may also form self-assembled structures with different morphologies.[30, 35, 36, 37] Amphiphilic multi-arm copolymers are more promising components of self-assembled materials compared to block copolymers due to their lower CMC and their ability to form stable assemblies.[23] While self-assembly of AB- and ABA-type amphiphilic block copolymers in the bulk is well studied both theoretically and experimentally,[38, 39, 40, 41, 42] systematic investigations on the effect of changes in macromolecular architectures on self-assembly structures have remained limited. In addition, precise structural analyses of self-assembly structures of star copolymers and cyclic copolymers are scarce, resulting in a lack of understanding of the conformation of polymer chains in self-assemblies.[43] Therefore, the effect of macromolecular architecture on self-assembly behavior has remained virtually unknown.

Herein, we report on the self-assembly behavior of four amphiphilic copolymers with different numbers of polymer chains, namely, AB, ABA, 3-arm block copolymers, and cyclic graft copolymers (**Fig. 1**). Our objective was to investigate the effect of changes in the macromolecular architecture on the self-assembly behavior and the conformation of polymer chains in the self-assemblies. Here, carbohydrates were used as the hydrophilic segment due to the few examples of amphiphilic glycopolymers where macromolecular architecture and self-assemblies have been investigated in detail. In this study, we chose maltopentaose and cycloamylose as the hydrophilic segments because of their high-water solubility and biodegradability. Our choice was based on previous our studies and in-depth knowledge of maltopentaose, particularly its size and structural behavior in self-assemblies.

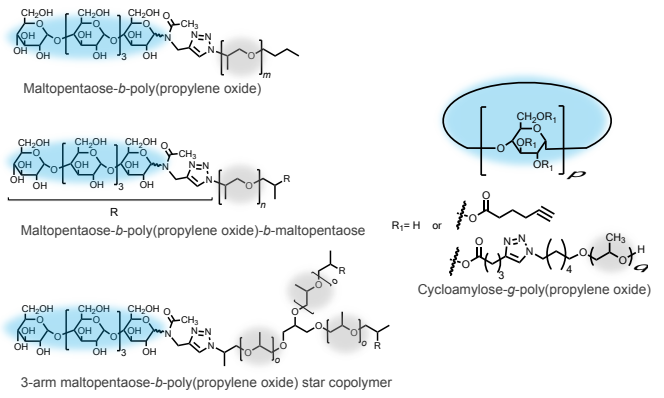

Fig. 1 Chemical structure of maltopentaose-*b*-PPO, maltopentaose-*b*-PPO-*b*-maltopentaose, 3-arm maltopentaose-*b*-PPO star copolymer, and cycloamylose-*g*-PPO.

In addition, the structure of cycloamylose in solution is well studied,[44] which also influenced our decision to use it as the hydrophilic segment. Thermoresponsive poly(propylene oxide)(PPO) was used as the hydrophobic segment. PPO is structurally similar to poly(ethylene glycol) and can hydrogen bond with water molecules. As a result, PPO exhibits lower critical solution temperature (LCST)-like behavior in aqueous solutions and is thus only soluble in cooled water (e.g., T_m < 18 °C for M_w = 2.0 × 10^3 g mol^{-1}).[45, 46] Furthermore, the phase transition temperature of PPO is known to depend on its molecular weight.[47] In this study, we used a set of PPOs whose molecular weights are sufficient to exhibit hydrophobicity at room temperature. As a characteristic related to the thermoresponsivity of PPO, we have previously reported that the hydrophobic regions of self-assemblies composed of amphiphilic polymers with PPO exhibit weakly hydrated states and can partition into not only hydrophobic but also hydrophilic compounds.[8, 48, 49, 50] Therefore, amphiphilic polymers with PPO would potentially be promising for the formation of polymer nanoreactors and drug carriers that can incorporate various substrates and drugs. Although the ratios of the molar mass of the hydrophilic part to the total molar mass of the polymers were comparable for all four copolymers, each polymer self-assembled, depending on the macromolecular architecture, into a different nanostructure, i.e., unilamellar vesicles, cylindrical micelles, spherical micelles, or multilamellar vesicles. We also show that the conformations of the polymer chains in the self-assemblies are different, as revealed by X-ray and light-scattering measurements, which results in the different nanostructures. Since changes in the morphology of amphiphilic polymers also change the structure of their self-assemblies, our findings contribute to the current understanding of the self-assembly behavior of amphiphilic multiarm copolymers and demonstrate the importance of the macromolecular architecture as a crucial factor in controlling the structure of molecular assemblies.

Results and discussion

In this study, we prepared amphiphilic glyco-copolymers with four different molecular architectures: (i) an AB block copolymer, (ii) an ABA block copolymer, (iii) a 3-arm AB block copolymer, and (iv) a cyclic graft copolymer. The block copolymers were synthesized by treating alkyne-functionalized maltopentaose with appropriate azide-functionalized poly(propylene oxide)s via a copper-catalyzed Huisgen cycloaddition reaction ('click chemistry'). Similarly, the cyclic graft copolymers were prepared by a coupling reaction between alkyne-functionalized cycloamylose and azide-functionalized PPO *via* click reactions. Detailed synthetic procedures are provided in the Supporting Information, along with representative ^{1}H NMR spectra, SEC chromatograms, and MALDI-TOF mass spectra (**Figs. S1–S10**). Given that the self-assembled structures vary as the ratio of the molar mass of the hydrophilic part to the total molar mass of the polymers ($f_{hydrophilic}$) changes,[51, 52] the ratio was kept constant throughout the experiments (*ca.* 0.31–0.36) in order to better understand the exclusive effect of the polymer architectures on the self-assembly behavior (**Table 1**).

Because the copolymers consist of thermoresponsive PPO, they were expected to exhibit phase-transition temperatures in aqueous solution. Accordingly, the thermoresponsive behavior of the corresponding copolymers in water was initially

Table 1 Molecular weights of the hydrophilic and hydrophobic segments of the copolymers and the ratio of the molar mass of the hydrophilic segment to the total molar mass of the copolymers

Polymer	molecular weight of the hydrophilic part (g mol^{-1})	molecular weight of the hydrophobic part (g mol^{-1})	the ratio of mass of the hydrophilic part to total mass
AB block copolymer	829	1.5×10^3	0.36
ABA block copolymer	829 × 2	3.4×10^3	0.33
3-arm AB block copolymer	829 × 3	4.5×10^3	0.36
Cyclic graft copolymer	4.2×10^3 [a]	9.3×10^3 [b]	0.31

a The molecular weight of cycloamylose was determined by MALDI TOF mass spectroscopy.

b The molecular weight was calculated by multiplying the molecular weight of PPO, the degree of the substitution of PPO and the degree of polymerization of cycloamylose.

investigated using pyrene fluorescence measurements to probe the formation of hydrophobic domains (**Fig. S11**). The I_1/I_3 values for all polymers gradually increased with decreasing solution temperature. The transition-temperature (T_m) values were determined from the maximum value of the first derivative of the I_1/I_3 values: the T_m values of the AB copolymer, ABA copolymer, 3-arm copolymer, and cyclic polymer are 18, 21, 25, and 9 °C, respectively. Although the ratios of the molar mass of the hydrophilic segments relative to the total molar mass of the polymers are comparable, significant differences were observed in their T_m values. The dramatic difference between the T_m values of the linear and cyclic graft polymers suggests that the thermoresponsive behavior is related to the molecular architecture. In general, the phase-transition temperature of polymers that exhibit LCST behavior decreases with increasing polymer concentration.[53, 54, 55] This is because the close proximity of the polymers facilitates intermolecular interactions during dehydration, resulting in a decrease in the T_m. The cyclic graft copolymers feature multiple thermoresponsive PPO chains within each molecule, thus increasing the apparent PPO concentration and reducing the T_m of the cyclic polymer compared to those of the other polymers.

Subsequently, we examined the effect of polymer architecture on the critical aggregation concentration (CAC) by employing 1,8-ANS, a fluorescence probe responsive to environmental changes. A decrease in polymer concentration corresponded with a decrease in fluorescence intensity (**Fig. S12**). The CAC values of AB, ABA, 3-arm block copolymers, and cyclic graft copolymers were determined to be 0.5, 0.5, 0.2, and 0.1 mg mL^{-1} respectively. We observed that the CAC values of the polymers decreased with an increase in the number of arms, suggesting that polymers with more arms facilitate self-assembly. This finding aligns with numerous studies reporting a similar trend, where an increase in the number of arms in both amphiphilic linear polymers and amphiphilic star polymers leads to a decrease in the CAC value.[23, 56, 57] This trend is attributed to the structural similarity between the unimer state and the micelle state of star block polymers with many arms, resulting in a reduced loss of transition entropy during micellization compared to linear block polymers. Based on these findings, we conclude that our polymers exhibit self-assembly behavior similar to that of the polymers studied in these reports.

Having confirmed the T_m values of the polymers, we then investigated the effect of the polymer architectures on the self-assembly behavior. The polymers were dissolved in water at a temperature of 0 °C, which is below the phase-transition temperature of all the polymers, and the resulting polymer solutions were incubated at 35 °C for at least 30 min. Dynamic light-scattering (DLS) analyses indicated average hydrodynamic radii of 55, 24, 8, and 57 nm for the AB copolymer, ABA copolymer, 3-arm copolymer, and cyclic polymer, respectively (**Table 2, Fig. S13**). The inconsistency among the particle sizes implies that the respective polymers form different molecular assemblies. We then carried out field-flow fractionation equipped with multi-angle light scattering (FFF-MALS; **Table 2**, **Fig. S14**) to obtain further structural information regarding the polymer assemblies. The molar masses of the assemblies were calculated to be 8.0×10^7, 6.9×10^6, 6.7×10^4, and 8.6×10^7 g mol^{-1} for the AB copolymer, ABA copolymer, 3-arm copolymer, and cyclic polymer, respectively. To gain insight into the self-assembly structures of the polymers, we performed transmission-electron-microscopy (TEM) measurements. TEM images of the AB polymer and cyclic polymer solution revealed spherical objects with an average size of 50–100 nm (**Figs. 2a and 2d**). The AB polymer assemblies exhibit circular boundaries with an average thickness of ~10 nm, suggesting that the assemblies are vesicular structures, whereas the cyclic polymer assemblies do not exhibit a clear boundary within the structures.

Table 2 Physical parameters of the self-assembled polymers in water

Polymer	R_h [a] (nm)	Molar mass [b] (g mol^{-1})	N_{agg}
AB block copolymer	55	8.0×10^7	3.6×10^4
ABA block copolymer	24	4.7×10^5	1.4×10^2
3-arm AB block copolymer	8	6.7×10^4	9.6
Cyclic graft copolymer	57	8.6×10^7	6.6×10^3

a The hydrodynamic radius was determined by DLS measurements.

b The molar mass was determined by SLS measurements.

These results indicate that these two self-assembly structures are different. The size and morphology of the ABA and 3-arm polymer assemblies are also completely different from those of the AB and cyclic polymer aggregates, with cylindrical assemblies (**Fig. 2b**) for the ABA polymer and spherical assemblies with an average size of ~15 nm for the 3-arm

polymer assemblies (**Fig. 2c**). Noted that we attempted to perform cryo-TEM observations on these assemblies. However, we encountered difficulties in maintaining the structural integrity of the assemblies during the cooling process. This resulted in the collapse of the assemblies and made meaningful imaging unfeasible. We then carried out small-angle X-ray scattering (SAXS) experiments to confirm the structures of the self-assemblies of the polymers. The scattering intensities in the low-q range decayed as a function of q^{-2} for the AB polymer (**Fig. 3a**), suggesting the presence of thin-plate-like structures. Using structural information from the TEM observations and the SAXS data, a cross-sectional bilayer model was found to fit well (**Fig. 3e**). In the scattering profile of the cyclic polymers, the slope of the scattering intensities was found to be a function of q^{-2} in the low-q range, and a Bragg peak at q = 0.66 nm^{-1} (d = 9.48 nm) was observed (**Fig. 3d**). As only the first peak was observed, the polymers are expected to form multilamellar vesicles with low periodicity. Therefore, we tried to fit the profile using a weakly ordered membrane-stack-particle model;[58, 59, 60] the fitting of this model to the profile was consistent with a hydrophilic thickness of 2.2 nm, a half-thickness of the hydrophobic layer of 2.4 nm, and a total bilayer number of 4 (**Fig. 3h, Tables 3 and S1**). Thus, the reason that the TEM images of the cyclic polymer solutions did not show clear boundaries, unlike the AB polymer assemblies (i.e., unilamellar vesicles), should be that the cyclic polymer assemblies form multilamellar vesicles, into which the TEM staining solution did not penetrate. On the other hand, the scattering intensities in the low-q range decayed as a function of q^{-1} and q^{0} for the ABA polymer and 3-arm polymer (**Figs. 3b and 3c**), which indicates the presence of rod-like structures and isolated particles, respectively. In fact, the SAXS profiles of the ABA polymer assemblies and 3-arm polymer assemblies could be fitted throughout almost the entire q-range by a core–shell cylinder model and a core–shell sphere model (**Figs. 3f and 3g, Table 3**). Overall, these results clearly demonstrate that the four polymers self-assemble into distinct self-assemblies, despite having comparable ratios of the molar mass of the hydrophilic segment to the total molar mass of the polymers.

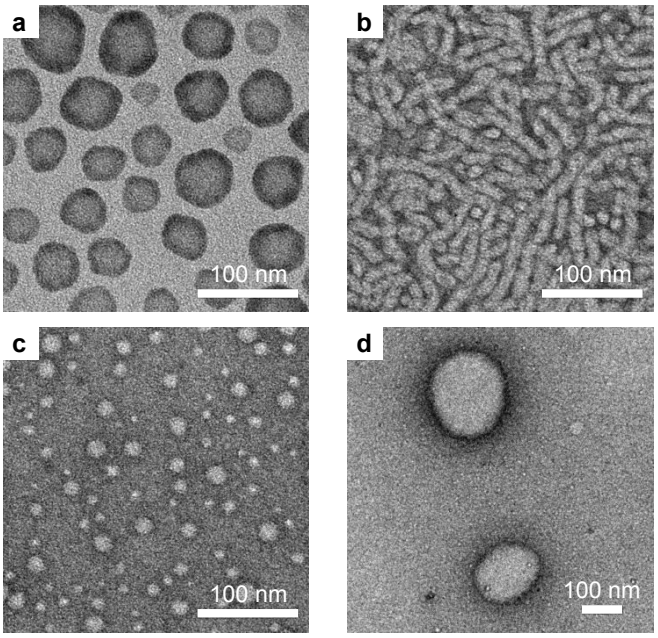

Fig. 2 TEM images of the self-assembled particles in the (a) AB block copolymer solution, (b) ABA block copolymer solution, (c) 3-arm AB block copolymer solution, and (d) cyclic graft copolymer solution using negative staining (phosphotungstic acid); [polymers] = 2.5 mg mL^{-1}.

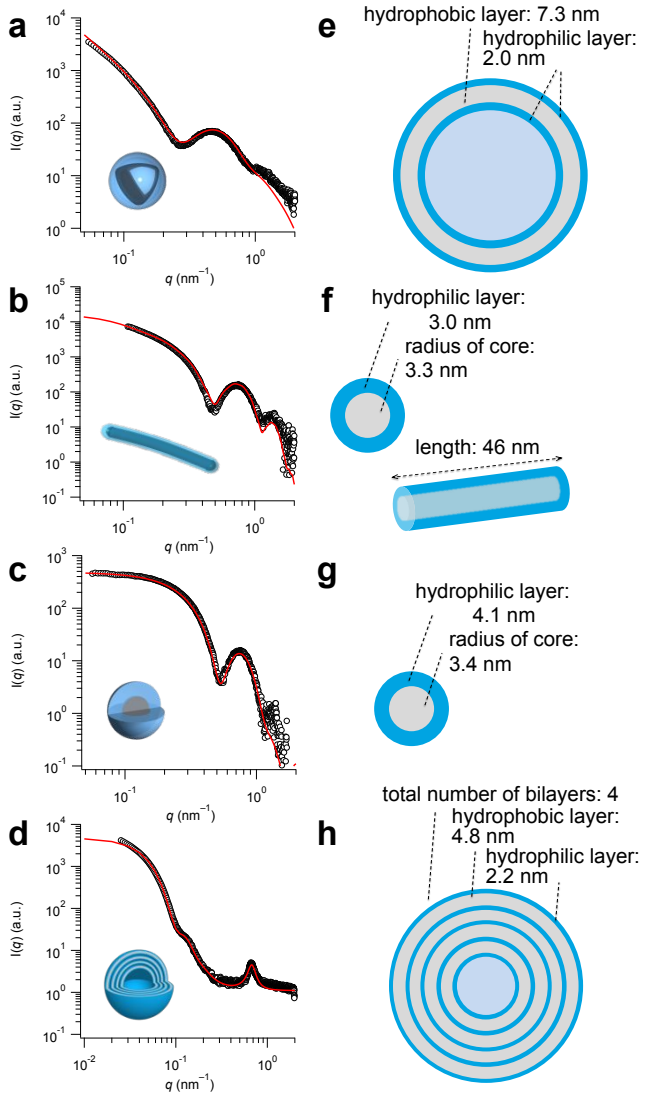

Fig. 3 SAXS profiles (open circles) of the self-assembled particles in the (a) AB block copolymer solution, (b) ABA block copolymer solution, (c) 3-arm AB block copolymer solution, and (d) cyclic graft copolymer solution. The red solid lines show the theoretical curves obtained using (a) bilayer cross-sectional, (b) core–shell cylinder, (c) core–shell sphere, and (d) weakly ordered membrane-stack-particle models. Representative structural parameters of the (e) spherical bilayer vesicles, (f) core–shell cylinder micelles, (g) core–shell spherical micelles, and (h) weakly ordered membrane-stack particles; [polymers] = 1.0 or 2.5 mg mL^{-1}.

An empirical rule based on the ratio of the molar mass of the hydrophilic part relative to the total molar mass of the polymers

($f_{hydrophilic}$) can predict the self-assembled structures of polymers; spherical micelles are formed when $f_{hydrophilic}$ is >45%; vesicles are favored when $f_{hydrophilic}$ is ~35%, and inverted nanostructures are formed when $f_{hydrophilic}$ is <25%.[51] Following this rule, we would expect the polymers to form vesicles, as they all have $f_{hydrophilic}$ values of ~30%. However, only the AB polymers and cyclic polymers formed vesicles. Consequently, the question arises of why the polymers self-assemble into different nanostructures even though their $f_{hydrophilic}$ values are almost identical. To answer this question, we tried to rationalize the geometric structures of the polymers in the assemblies by calculating the apparent critical-packing parameters (cpp). For this purpose, we used the degree of substitution of PPO, the aggregation number, and the fitting parameters obtained from the SAXS analyses.[61, 62] The apparent cpp values of the AB polymer, ABA polymer, 3-arm polymer, and cyclic polymer were calculated to be 1.05, 0.47, 0.33, and 0.99, respectively (**Table 4**; for details of the calculations, see the Supporting Information). The ABA polymers and 3-arm polymers were found to have cpp values that are different to those of the AB polymers and cyclic polymers. Generally, when 0 < cpp ≤ 1/3, spherical micelles form. If 1/3 < cpp ≤ 1/2, then cylindrical structures are predominantly formed, whereas amphiphiles self-assemble into vesicular structures when 1/2 < cpp ≤ 1.[17] The geometry of the different polymer self-assemblies was generally in accordance with those predicted from their calculated cpp values.

Table 3 Fitting parameters of the self-assemble polymers obtained from SAXS analyses

AB block copolymer		thickness of the hydrophilic region (nm)	thickness of the hydrophobic region (nm)	electron density of core (e nm^{-3})	electron density of shell (e nm^{-3})
		2.0	7.3	325	382
ABA block copolymer	radius of core (nm)	overall radius of micelles (nm)	half length of micelles (nm)	electron density of core (e nm^{-3})	electron density of shell (e nm^{-3})
	3.3	6.3	23	329	380
3-arm AB block copolymer		radius of core (nm)	overall radius of micelles (nm)	electron density of core (e nm^{-3})	electron density of shell (e nm^{-3})
		3.4	7.5	310	375
Cyclic graft copolymer	total number of bilayer	thickness of the hydrophilic region (nm)	thickness of the hydrophobic region (nm)	electron density of core (e nm^{-3})	electron density of shell (e nm^{-3})
	4	2.2	4.8	337	369

Table 4 Structural parameters of the self-assembled polymers for determining the critical packing parameters (cpps)

Polymer	v (nm^3)	a (nm^2)	l (nm)	cpp
AB block copolymer	7.1	1.8	3.7	1.05
ABA block copolymer	5.6	3.7	3.3	0.47
3-arm AB block copolymer	5.7	5.0	3.4	0.33
Cyclic graft copolymer	7.0	2.9	2.4	0.99

Interestingly, the cross-sectional area of the hydrophilic region per amphiphilic unit (a) increases with increasing number of PPO arms (1.8–4.7 nm^2), except in the case of the cyclic graft copolymer assemblies. Although each polymer contains the same amphiphilic units, the different values of a indicate that the amphiphilic units are packed differently in the respective self-assembled structures. Star polymers tend to adopt a configuration in which each polymer chain gathers around the tether-branching point rather than spreading out from the branching point, in order to reduce conformational entropy loss.[56, 63] However, due to the steric hindrance that exists between the polymer chains within the molecule, the star-polymer chains are unable to pack tightly together and instead adopt a slightly spread-out shape (**Fig. S15**). For ABA triblock copolymer assemblies, the polymer chain can adopt either a loop comformation, where the B block bends, or a bridge conformation, in which the B block straightens across the core of the assembly.[64, 65] In our case, the cross-sectional area of the hydrophilic region of ABA polymer assembly is larger than that of AB polymer assembly, suggesting that the PPO chain in the ABA polymers might asssume the formation of a loop-like structure. If this is the case, the ABA polymers would be expected to fold in half; due to their reduced number of polymer chains compared to the 3-arm polymers, the effect of steric hindrance is less pronounced, allowing them to fold more tightly than the 3-arm polymers, and therefore to exhibit lower hydrophilic region surface area (a). For the graft copolymer self-assemblies, the hydrophilic backbone, which is sandwiched between the hydrophobic side chains, folds to form a loop-like structure. Due to the persistence length of the main chain and the exclusion-volume effects between the main chain in the loop-like structure, it is difficult for it to fold compactly. Therefore, the cyclic graft copolymers have a slightly higher a value. Conversely, the AB polymers, which have no intramolecular steric hindrance, exhibited the lowest value of a among the four polymers.

Unlike the cross-sectional area of the hydrophilic region per amphiphilic unit, the volumes of the hydrophobic region per amphiphilic unit (v) are independent of the number of arms. The AB block copolymers and cyclic copolymers have large v values. Both polymers form vesicles, and therefore, the v values likely correlate with the conformation of PPO in the self-assemblies.

The ABA triblock copolymers and 3-arm AB block copolymers form hydrophobic regions by folding the PPO chains, resulting in a suppression of PPO chain motion. In contrast, the AB block copolymers and cyclic graft copolymers have PPO chains that are attached to hydrophilic segments at only one end, allowing them to be more mobile than those of the ABA triblock copolymers and 3-arm copolymers. This difference in mobility is thought to be a factor in the difference in the *v* values.

In the self-assembly of amphiphilic graft copolymers, the surface area of the hydrophilic region depends on the flexibility (persistence length; *p*) of the backbone chain, which forms the hydrophilic domain by folding.[61, 66] A longer persistence length results in a more rigid and less flexible chain, while a shorter persistence length results in a more flexible and softer chain. We have reported that the formation of vesicles occurs when the persistence length *p* of the main chain in graft polymers is <2 nm, rod-shaped aggregates are formed for 2 nm < *p* < 2.7 nm, and spherical aggregates are formed for *p* > 2.9 nm.[62] Thus, the nanostructures of graft copolymer assemblies can be controlled by adjusting the persistence length of the main chain. Cycloamylose has a persistence length of ~2 nm, which makes it a flexible polymer that can fold compactly when used as a main chain of graft copolymers.[67] In agreement with the aforementioned empirical rule, the cyclic graft copolymer in this study self-assembled into vesicles. The difference between the present cyclic graft copolymer and previously reported graft copolymers is that this cyclic graft copolymer formed multilamellar vesicles. Song *et al*. have reported that multilamellar vesicles can be formed using amphiphilic copolymers with hydrophilic blocks that do not have sufficient hydrophilicity to completely dissolve and stabilize the bilayer.[68] From the SAXS analysis of the cyclic copolymer assemblies (**Table 3**), we can estimate a total bilayer thickness (*l* = 9.2 nm), which is the sum of the thickness of the hydrophilic layer (2.2 nm × 2) and the hydrophobic layer (4.8 nm). The value of *l* is almost the same as the *d*-spacing (9.48 nm) calculated from the Bragg peak at q = 0.66 nm^{-1}; the *d*-spacing is the thickness including the thickness of the bilayer and the hydration layer. The fact that the *d*-spacing and the total bilayer thickness *l* are virtually identical suggests that the structure is a dehydrated multilayer stack. In addition, cyclic graft polymers with a lower degree of PPO substitution were also able to form multilamellar vesicles (**Fig. S16**), suggesting that the main chains are not sufficiently hydrated to dissolve the bilamellar membrane. In contrast to pullulan and dextran, cycloamylose adapts a helical structure in aqueous solution, and the helix structure of polysaccharides is stabilized by intramolecular hydrogen bonding between the hydroxy groups of the carbohydrate groups. This leads to a decrease in the number of hydrogen bonds between the carbohydrate groups and water, resulting in dehydration of the polysaccharide chain. For example, for cycloamylose, which adopts a helical configuration, it has been observed that each glucose unit is hydrogen-bonded to 4.6 molecules of water.[69] Curdlan forms a triple helical structure, in which two water molecules are hydrogen-bonded to each molecule.[70] In contrast, hyaluronan and dextran, which do not exhibit helical structures, have been reported to form 6–7.5 hydrogen bonds per monosaccharide,[71] and polysaccharides that do not form a helix are hydrated. We therefore sought to confirm the formation of cycloamylose helices in the molecular assemblies. The inner cavity of the cycloamylose helix is a hydrophobic space that is able to encapsulate hydrophobic species such as iodide ions.[72, 73] To confirm its encapsulation ability, we mixed cycloamylose-g-PPO solution with a solution of KI and I_2 and measured the UV-vis spectrum of the resulting solution (**Fig. S17**). The UV-vis spectrum of the solution showed a peak at 353 nm, which was attributed to I_3^- ions, and the absorbance of this peak decreased with increasing concentration of cycloamylose-*g*-PPO. In addition, the peak at 353 nm shifted to 357 nm. These spectral changes are in good agreement with those previously reported for the encapsulation of the I_3^- ion in host molecules such as cyclodextrin.[74, 75] Alkyne-functionalized cycloamylose also showed a similar hypochromic effect and red shift, suggesting that the I_3^- ion is encapsulated within the helix and not in the PPO layer. These results clearly indicate the encapsulation of I_3^- ions by the main-chain cycloamylose in the assemblies. Thus, the formation of helices by cycloamylose would result in a decrease in main-chain hydration and prevent the complete dissolution of the bilayer, resulting in the formation of multilamellar vesicles.

In the present work, we used PPO, which has a low glass-transition temperature[76, 77] and thus allows it to fold flexibly and form different self-assemblies for each polymer. It is expected that the use of bulky or less flexible hydrophobic chains would result in different self-assembly behavior. We are currently working on investigating the relationship between the flexibility of the hydrophobic chains and the nanostructures of self-assemblies to reveal the generality of these results using polymers other than PPO; the corresponding results will be reported elsewhere in due course.

Overall, the results of this study indicate that changes in the molecular architecture of amphiphilic copolymers can lead to substantial changes in the structure of their self-assemblies, even when the weight fractions of the hydrophilic and hydrophobic segments of the amphiphilic molecules are kept constant. In addition, when attempting to obtain a specific molecular-assembly structure using branched amphiphilic polymers, it is imperative to carefully design the molecular architecture, taking into account the folding of the polymer chains.

Conclusions

In summary, we report that four amphiphilic copolymers with comparable ratios of the molar mass of the hydrophilic segment to the total molar mass of the polymer self-assemble into spherical micelles, cylindrical micelles, or vesicles depending on the polymer architecture. This different self-assembly behavior is mainly caused by the differences in the folding of the multi-armed hydrophobic segments, which results in different surface areas of the hydrophilic region of the amphiphilic units of the polymers. Consequently, the polymers self-assemble into different morphologies. Studies of surfactant and block

copolymer self-assemblies have so far mainly focused on the relative molecular weights of the hydrophilic and hydrophobic segments as a means to control the morphologies of the resulting self-assemblies. However, in multi-arm amphiphilic copolymer self-assemblies, the folding of the polymer chain should be considered in addition to other molecular-structure factors in order to generate molecular assemblies with a targeted morphology. This study sheds light on the influence of the macromolecular architecture on the self-assembly behavior of non-AB -type amphiphilic copolymers and adds to the current understanding of the field of polymer self-assembly. This study can thus be expected to allow the development of novel design approaches for multi-arm copolymers that enable the fabrication of molecular assemblies with controlled nanostructures.

Author Contributions

The manuscript was written through contributions of all authors. All authors have given approval to the final version of the manuscript.

Conflicts of interest

There are no conflicts to declare.

Acknowledgements

This work was supported by the JSPS in the form of grants-in-aid for scientific research (B:22H02140, Exploratory:22K19057), the MEXT Leading Initiative for Excellent Young Researchers, the JST FOREST Program (JPMJFR201P), and the MEXT Promotion of Distinctive Joint Research Center Program (JPMXP0621467946). SAXS experiments were conducted at the BL40B2 beamline of SPring-8 under proposal numbers 2021A1065, 2021B1089, 2022A1095, 2022B1109, and 2023A1121.

References

1. V. Percec, C. H. Ahn, G. Ungar, D. J. P. Yeardley, M. Möller and S. S. Sheiko, *Nature*, 1998, **391**, 161-164.
2. C. Chen, R. A. L. Wylie, D. Klinger and L. A. Connal, *Chem. Mater.*, 2017, **29**, 1918-1945.
3. L. MacFarlane, C. Zhao, J. Cai, H. Qiu and I. Manners, *Chem. Sci.*, 2021, **12**, 4661-4682.
4. S. Ganda and M. H. Stenzel, *Prog. Polym. Sci.*, 2020, **101**, 101195.
5. T. Smart, H. Lomas, M. Massignani, M. V. Flores-Merino, L. R. Perez and G. Battaglia, *Nano Today*, 2008, **3**, 38-46.
6. Z. L. Tyrrell, Y. Shen and M. Radosz, *Prog. Polym. Sci.*, 2010, **35**, 1128-1143.
7. E. A. Scott, A. Stano, M. Gillard, A. C. Maio-Liu, M. A. Swartz and J. A. Hubbell, *Biomaterials*, 2012, **33**, 6211-6219.
8. T. Nishimura, Y. Sasaki and K. Akiyoshi, *Adv. Mater.*, 2017, **29**, 1702406.
9. R. Ruiz, H. Kang, F. A. Detcheverry, E. Dobisz, D. S. Kercher, T. R. Albrecht, J. J. de Pablo and P. F. Nealey, *Science*, 2008, **321**, 936-939.
10. N. McGrath, A. J. Patil, S. M. D. Watson, B. R. Horrocks, C. F. J. Faul, A. Houlton, M. A. Winnik, S. Mann and I. Manners, *Chem. Euro. J.*, 2013, **19**, 13030-13039.
11. Y. Geng, P. Dalhaimer, S. Cai, R. Tsai, M. Tewari, T. Minko and D. E. Discher, *Nat. Nanotechnol.*, 2007, **2**, 249-255.
12. E. Blanco, H. Shen and M. Ferrari, *Nat. Biotechnol.*, 2015, **33**, 941-951.
13. X. Hu, J. Hu, J. Tian, Z. Ge, G. Zhang, K. Luo and S. Liu, *J. Am. Chem. Soc.*, 2013, **135**, 17617-17629.
14. Q. Shi, H. Yin, R. Song, J. Xu, J. Tan, X. Zhou, J. Cen, Z. Deng, H. Tong, C. Cui, Y. Zhang, X. Li, Z. Zhang and S. Liu, *Nat. Chem.*, 2023, **15**, 257-270.
15. Q.-Q. Shi, X. Zhou, J. Xu, N. Wang, J.-L. Zhang, X.-L. Hu and S.-Y. Liu, *Chin. J. Polym. Sci.*, 2023, **41**, 768-777.
16. R. Nagarajan, *Langmuir*, 2002, **18**, 31-38.
17. J. N. Israelachvili, D. J. Mitchell and B. W. Ninham, *J. Chem. Soc., Fraday Trans. 2*, 1976, **72**, 1525-1568.
18. M. Antonietti and S. Förster, *Adv. Mater.*, 2003, **15**, 1323-1333.
19. A. Blanazs, S. P. Armes and A. J. Ryan, *Macromol. Rapid. Commun.*, 2009, **30**, 267-277.
20. Y. Zhang, T. Guan, G. Han, T. Guo and W. Zhang, *Macromolecules*, 2019, **52**, 718-728.
21. K. Hu, J. Sarkar, J. Zheng, Y. H. M. Lim and A. Goto, *Macromol. Rapid. Commun.*, 2020, **41**, 2000075.
22. H. Liu, J. Xu, J. Jiang, J. Yin, R. Narain, Y. Cai and S. Liu, *J. Polym. Sci., Part A: Polym. Chem.*, 2007, **45**, 1446-1462.
23. K. H. Kim, G. H. Cui, H. J. Lim, J. Huh, C.-H. Ahn and W. H. Jo, *Macromol. Chem. Phys.*, 2004, **205**, 1684-1692.
24. T. Yamamoto and Y. Tezuka, *Soft Matter*, 2015, **11**, 7458-7468.
25. R. J. Williams, A. P. Dove and R. K. O'Reilly, *Polym. Chem.*, 2015, **6**, 2998-3008.
26. S. Honda, T. Yamamoto and Y. Tezuka, *Nat. Commun.*, 2013, **4**, 1574.
27. S. Honda, T. Yamamoto and Y. Tezuka, *J. Am. Chem. Soc.*, 2010, **132**, 10251-10253.
28. C. Burguière, C. Chassenieux and B. Charleux, *Polymer*, 2003, **44**, 509-518.
29. X.-H. Dai and C.-M. Dong, *J. Polym. Sci., Part A: Polym. Chem.*, 2008, **46**, 817-829.
30. T. Isono, K. Miyachi, Y. Satoh, R. Nakamura, Y. Zhang, I. Otsuka, K. Tajima, T. Kakuchi, R. Borsali and T. Satoh, *Macromolecules*, 2016, **49**, 4178-4194.
31. M. R. Whittaker and M. J. Monteiro, *Langmuir*, 2006, **22**, 9746-9752.
32. S. Pispas, N. Hadjichristidis, I. Potemkin and A. Khokhlov, *Macromolecules*, 2000, **33**, 1741-1746.
33. K. Sotiriou, A. Nannou, G. Velis and S. Pispas, *Macromolecules*, 2002, **35**, 4106-4112.
34. G. Mountrichas, M. Mpiri and S. Pispas, *Macromolecules*, 2005, **38**, 940-947.
35. R. Borsali, E. Minatti, J.-L. Putaux, M. Schappacher, A. Deffieux, P. Viville, R. Lazzaroni and T. Narayanan, *Langmuir*, 2003, **19**, 6-9.
36. Y. Zhang, M. Cao, G. Han, T. Guo, T. Ying and W. Zhang, *Macromolecules*, 2018, **51**, 5440-5449.
37. B. Zhang, H. Zhang, Y. Li, J. N. Hoskins and S. M. Grayson, *ACS Macro Lett.*, 2013, **2**, 845-848.
38. Y. Mai and A. Eisenberg, *Chem. Soc. Rev.*, 2012, **41**, 5969-5985.
39. S. B. Darling, *Prog. Polym. Sci.*, 2007, **32**, 1152-1204.
40. N. A. Lynd, A. J. Meuler and M. A. Hillmyer, *Prog. Polym. Sci.*, 2008, **33**, 875-893.
41. M. Karayianni and S. Pispas, *J. Polym. Sci.*, 2021, **59**, 1874-1898.
42. I. W. Hamley, *Nanotechnology*, 2003, **14**, R39.

43. R. J. Williams, A. Pitto-Barry, N. Kirby, A. P. Dove and R. K. O'Reilly, *Macromolecules*, 2016, **49**, 2802-2813.
44. K. Gessler, I. Usón, T. Takaha, N. Krauss, S. M. Smith, S. Okada, G. M. Sheldrick and W. Saenger, *Proc. Natl. Acad. Sci. USA*, 1999, **96**, 4246-4251.
45. K. Mortensen and J. S. Pedersen, *Macromolecules*, 1993, **26**, 805-812.
46. K. Mortensen and W. Brown, *Macromolecules*, 1993, **26**, 4128-4135.
47. J. Armstrong, B. Chowdhry, R. O'Brien, A. Beezer, J. Mitchell and S. Leharne, *J. Phys. Chem.*, 1995, **99**, 4590-4598.
48. T. Nishimura, L. de Campo, H. Iwase and K. Akiyoshi, *Macromolecules*, 2020, **53**, 7546-7551.
49. T. Nishimura, S. Shishi, Y. Sasaki and K. Akiyoshi, *J. Am. Chem. Soc.*, 2020, **142**, 11784-11790.
50. T. Nishimura, S. Hirose, Y. Sasaki and K. Akiyoshi, *J. Am. Chem. Soc.*, 2020, **142**, 154-161.
51. D. E. Discher and A. Eisenberg, *Science*, 2002, **297**, 967-973.
52. H. Aranda-Espinoza, H. Bermudez, F. S. Bates and D. E. Discher, *Phys. Rev. Lett.*, 2001, **87**, 208301.
53. J.-F. Lutz, Ö. Akdemir and A. Hoth, *J. Am. Chem. Soc.*, 2006, **128**, 13046-13047.
54. P. Kujawa, F. Segui, S. Shaban, C. Diab, Y. Okada, F. Tanaka and F. M. Winnik, *Macromolecules*, 2006, **39**, 341-348.
55. K. Bebis, M. W. Jones, D. M. Haddleton and M. I. Gibson, *Polym. Chem.*, 2011, **2**, 975-982.
56. H. J. Lim, H. Lee, K. H. Kim, J. Huh, C.-H. Ahn and J. W. Kim, *Colloid Polym. Sci.*, 2013, **291**, 1817-1827.
57. J. Cao, A. Lu, C. Li, M. Cai, Y. Chen, S. Li and X. Luo, *Colloids Surf. B: Biointerfaces*, 2013, **112**, 35-41.
58. G. Pabst, M. Rappolt, H. Amenitsch and P. Laggner, *Phys. Rev. E*, 2000, **62**, 4000-4009.
59. V. Castelletto, G. Cheng, C. Stain, C. J. Connon and I. W. Hamley, *Langmuir*, 2012, **28**, 11599-11608.
60. K. Aburai, K. Hatanaka, S. Takano, S. Fujii and K. Sakurai, *Langmuir*, 2020, **36**, 12545-12554.
61. T. Nishimura, S. Fujii, K. Sakurai, Y. Sasaki and K. Akiyoshi, *Macromolecules*, 2021, **54**, 7003-7009.
62. T. Nishimura, Y. Hatatani, M. Ando, Y. Sasaki and K. Akiyoshi, *Chem. Sci.*, 2022, **13**, 5243-5251.
63. J. Xu and E. R. Zubarev, *Angew. Chem., Int. Ed.*, 2004, **43**, 5491-5496.
64. A. Prhashanna and S. B. Chen, *Polymer*, 2017, **118**, 22-29.
65. J. Huh, W. H. Jo and G. ten Brinke, *Macromolecules*, 2002, **35**, 2413-2416.
66. Y. Sakamoto and T. Nishimura, *Polym. Chem.*, 2022, **13**, 6343-6360.
67. Y. Nakata, K. Amitani, T. Norisuye and S. Kitamura, *Biopolymers*, 2003, **69**, 508-516.
68. Z. Song, H. Kim, X. Ba, R. Baumgartner, J. S. Lee, H. Tang, C. Leal and J. Cheng, *Soft Matter*, 2015, **11**, 4091-4098.
69. S. Kitamura, H. Isuda, J. Shimada, T. Takada, T. Takaha, S. Okada, M. Mimura and K. Kajiwara, *Carbohydr. Res.*, 1997, **304**, 303-314.
70. C. T. Chuah, A. Sarko, Y. Deslandes and R. H. Marchessault, *Macromolecules*, 1983, **16**, 1375-1382.
71. J. Hunger, A. Bernecker, Huib J. Bakker, M. Bonn and Ralf P. Richter, *Biophys. J.*, 2012, **103**, L10-L12.
72. J. Wang, A. Jiao, Y. Tian, X. Xu, Z. Jin and Y. Li, *J. Chromatogr. A*, 2011, **1218**, 863-868.
73. O. Nimz, K. Gessler, I. Usón, G. M. Sheldrick and W. Saenger, *Carbohydr. Res.*, 2004, **339**, 1427-1437.
74. J. L. Pursell and C. J. Pursell, *J. Phys. Chem. A*, 2016, **120**, 2144-2149.
75. Y. Liang, J. Ka-Ho Hui, M.-a. Morikawa, H. Inoue, T. Yamada and N. Kimizuka, *ACS Appl. Energy Mater.*, 2021, **4**, 5326-5331.
76. J. Herzberger, K. Niederer, H. Pohlit, J. Seiwert, M. Worm, F. R. Wurm and H. Frey, *Chem. Rev.*, 2016, **116**, 2170-2243.
77. R. Klein and F. R. Wurm, *Macromol. Rapid. Commun.*, 2015, **36**, 1147-1165.